Korean J. Chem. Eng., 37(12), 2216-2224 (2020)
DOI: 10.1007/s11814-020-0640-0

pISSN: 0256-1115
eISSN: 1975-7220

Simultaneous biosynthesis of reduced graphene oxide-Ag-Cu_2O nanostructures by lichen extract for catalytic reduction of textile dyes

Zafer Çıplak*, Bengü Getiren*, Ceren Gökalp*, Ceren Atila Dinçer*,†, Atila Yıldız, and Nuray Yıldız***

*Department of Chemical Engineering, Ankara University, 06100, Tandoğan, Ankara, Turkey
**Department of Biology, Ankara University, 06100, Tandoğan, Ankara, Turkey
(*Received 20 March 2020 • Revised 8 July 2020 • Accepted 14 July 2020*)

Abstract–Metal/metal oxide nanostructures based reduced graphene oxide (LrGO-Ag, LrGO-Cu_2O, LrGO-Ag-Cu_2O) nanocomposites were obtained via green method using *Cetraria islandica* (L.) Ach. lichen extract. Fourier transform infrared (FTIR) spectroscopy, transmission electron microscopy (TEM), scanning electron microscope energy-dispersive X-ray spectroscopy (SEM–EDX), ultraviolet-visible (UV-Vis) spectroscopy, X-ray diffraction (XRD) and X-ray photoelectron spectroscopy (XPS) were performed to analyze the prepared nanostructures. The results indicated that the nanocomposites were synthesized effectively and Ag-Cu_2O nanoparticles with the mean diameter of 27 nm were well dispersed on the LrGO. The conversion of methylene blue (MB) to Leuco Methylene Blue (LMB) and 4-Nitrophenol (4-NP) to 4-Aminophenol (4-AP) was performed by biosynthesized catalysts in the presence of $NaBH_4$. The reaction rate of LrGO-Ag-Cu_2O nanocomposite during 4-NP and MB reduction was found as 0.0026 s^{-1} and 0.0497 s^{-1}, respectively. The LrGO-Ag-Cu_2O nanocomposite showed superior catalytic performance for the reduction of both textile dyes.

Keywords: Metal/Metal Oxide Nanostructures, Reduced Graphene Oxide (rGO), *Cetraria islandica* (L.) Ach. Extract, Green Synthesis, Catalytic Reduction

INTRODUCTION

Water pollution caused by textile dyes is an important problem worldwide [1]. Several methods, such as biodegradation [2], chemical and electrochemical oxidation [3], chemical coagulation [4], membrane filtration [5], and adsorption [6] can be used to remove dyes from water. However, these methods have some drawbacks like high cost, the phase change of pollution, and excess sludge. To overcome these drawbacks, catalytic reduction of dyes with metal nanoparticles (Ag, Cu, Ni, Au…) is suggested as an effective alternative method [7-9]. Metal nanoparticles (MNPs) exhibit superior optic, electronic and magnetic properties different from their bulk structures. On the other hand, metal-metal oxide nanoparticles have favorable attributes by the reason of the synergistic effects of the components [10,11]. Cu_2O is a p-type semiconductor metal oxide which has drawn considerable interest due to its catalytic, optical and electronic properties. It has low toxicity, low-cost, and abundance [12-14]. Especially, because of being inexpensive and suitable for large scale production, Cu_2O is a promising alternative to expensive rare metal nanoparticles (Pt, Au, Ag and Pd) towards catalytic applications [15]. On the other hand, previous researches have exhibited nanocomposites of Cu_2O-noble metal nanoparticles (Pd, Ag, Au and Pt) [12,16-18] and Cu_2O-carbonaceous structures reduced graphene oxide [13,15,19], amine-functionalized graphite [20] and cubic ordered mesoporous carbon [21] which have excellent catalytic properties. Sol-gel, chemical and electrochemical reduction, chemical precipitation, micro emulsion, pyrolysis and solvothermal methods for the synthesis of metal/metal oxide nanoparticles are expensive and include toxic chemicals. Therefore, researchers have focused on green synthesis methods that are non-toxic, low-cost and environmentally friendly. Lichen extract mediated synthesis is one of the green synthesis methods [22-26]. Lichens are a symbiotic relationship of photobionts and mycobionts. *Cetraria islandica* (L.) Ach. which is a widespread lichen type especially in the Northern European countries and also Central Anatolia of Turkey, including - isolichenan polysaccharides and lichesterinic acid - protolichesterinic acid - roccellaric acid - fumarprotocetraric acid - protocetraric acid secondary metabolites [27-30].

Metal nanostructures can be utilized as catalysts by synthesizing a nanocomposite with graphene or graphene based structures like graphene oxide (GO) and reduced graphene oxide (rGO).

Graphene is a two-dimensional material composed of sp^2 hybridized carbon atoms with high specific surface area, high crystallinity and electronic property. This superior material and its derivatives possess wide application areas like batteries, supercapacitors, drug delivery, antibacterial and catalysis. Because of having very high surface area and inert structure, rGO is a useful platform to achieve stable metal and metal oxide nanostructures especially to enhance catalytic activity [31-33].

A heterocyclic aromatic dye Methylene Blue (MB) and an aromatic nitro compound 4-Nitrophenol (4-NP) are toxic and hazardous materials for environment and human health. Due to the negative properties of these textile dyes, catalytic reduction of MB and 4-NP has been widely investigated. Leuco Methylene Blue (LMB) and 4-Aminophenol (4-AP) are the reduction products of MB and 4-NP, respectively. LMB is a colorless hydrogenated mole-

†To whom correspondence should be addressed.
E-mail: catila@eng.ankara.edu.tr

cule used in holographic industries and data recording [34] and 4-AP can be used as an active agent to prepare antipyretic and analgesic drugs [35-37].

There are several studies related to reduction of the textile dyes by rGO based metal/metal oxide nanostructures (Ag/rGO/TiO_2, [38]; Pd/rGO/Fe_3O_4, [39]; Au-Cu/rGO, [40]; Ag/$CuFe_2O_4$/rGO, [41]).

In the present study, a hybrid of Cu_2O (metal oxide nanoparticles), Ag (noble metal nanoparticles), and rGO was attained with a facile, a single-step approach. GO, $AgNO_3$, and $CuSO_4 \cdot 5H_2O$ were reduced simultaneously with *C. islandica* extract, which also undertakes the stabilizing agent role. Because of being an effective reducing agent, *C. islandica* extract provides one-pot and simultaneous reduction of GO and metal/metal oxide precursors, for preparation of ternary LrGO-Ag-Cu_2O nanocomposite. In addition, as an effective stabilizing agent, *C. islandica* extract improves dispersibility and processability to maintain the effective surface area of the rGO nanosheets, and coating of the surface of rGO nanosheets homogeneously with metal/metal oxide nanoparticles [42]. Additionally, although most of the phytoextracts used in chemical reduction of GO and metal salts are only available in certain locations, *C. islandica* is a lichen type available in many parts of the world [28,43]. LrGO-Ag, LrGO-Cu_2O, LrGO-Ag-Cu_2O nanostructures were synthesized with a green method using *C. islandica* extract acting as both reducing and stabilizing agent. This is the first study on the synthesis and investigation of catalytic activity of LrGO-Cu_2O and LrGO-Ag-Cu_2O nanostructures obtained by lichen extract to the best of our knowledge so far.

MATERIALS AND METHODS

1. Materials

The Lichen *C. islandica* was gathered in the Yapraklı, Çankırı region from Turkey. Graphite oxide with 1.5 nm thickness, 50 μm mean diameter was provided from Grafen Chemical Industries Co., Turkey. Silver nitrate ($AgNO_3$, ≥99.5%, Sigma Aldrich), copper (II) sulfate pentahydrate ($CuSO_4 \cdot 5H_2O$, for analysis EMSURE® ACS, ISO, Reag. Ph Eur, Merck), sodium hydroxide (NaOH, reagent grade ≥98%, Sigma), sodium borohydride ($NaBH_4$, fine granular for synthesis, Merck), 4-Nitrophenol (4-NP, reagent grade ≥98% for synthesis, Merck), methylene blue (MB, for Reag. Ph Eur, Merck) were used for the synthesis of nanostructures and determination of their catalytic activities.

2. Preparation of *C. islandica* Extract

C. islandica was used in the synthesis of LrGO-Ag, LrGO-Cu_2O, LrGO-Ag-Cu_2O nanostructures. The lichen was cleaned under a microscope and subjected to size reduction with liquid nitrogen prior to extraction process with ethanol.

3. Preparation of LrGO-Ag-Cu_2O Nanocomposites

LrGO based nanocomposites (LrGO-Ag, LrGO-Cu_2O, LrGO-Ag-Cu_2O) were prepared with simultaneous reduction of GO, $CuSO_4$ and $AgNO_3$. 25 mg of graphite oxide was exfoliated in 50 ml of DI water to obtain GO dispersion by sonication for 1 h (Elmasonic S 70 H, 150 W, 47 kHz). $AgNO_3$ and $CuSO_4 \cdot 5H_2O$ solutions were added to obtained dispersion (1 : 1, n/n) and the mixtures were sonicated for another 1 h. 6 ml lichen extract and 1.5 ml NaOH solution (0.5 M) were added dropwise to the above mixture at 95 °C under constant stirring and reflux. At specific time intervals, samples were analyzed by UV-Vis, thus the reaction time was determined as 2 h. The solutions of LrGO based Ag-Cu_2O nanocomposites were filtered, washed with DI water and ethanol several times and dried under vacuum at 60 °C. Nanomaterials containing Cu_2O were synthesized under nitrogen atmosphere.

4. Characterization of Nanostructure

The synthesized nanostructures were analyzed with Fourier-transform infrared spectroscopy (FTIR, 8400 S Shimadzu) with a scan interval 400 cm^{-1} to 4,000 cm^{-1} using KBr pressed disks, trans-

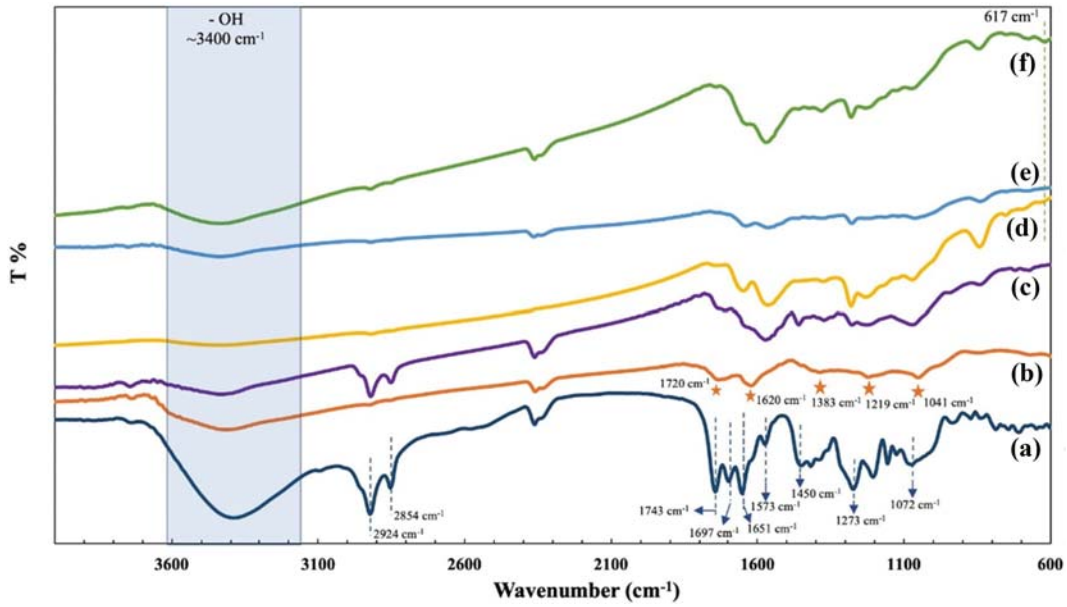

Fig. 1. FTIR spectra of (a) *Cetraria islandica* (L.) Ach. extract, (b) GO, (c) LrGO, (d) LrGO-Cu_2O, (e) LrGO-Ag and (f) LrGO-Ag-Cu_2O nanostructures.

mission electron microscopy (TEM, FEI Tecnai G2) operating at 120 kV, scanning electron microscopy (SEM-SEM/EDX, FEI QUANTA 400F). For SEM analysis the samples were drop coated onto an Al foil covered stub, X-ray diffraction (XRD, Rigaku Ultima-IV) with a scanning rate 2°/min and scan interval 20° to 80°, and X-ray photoelectron spectroscopy (XPS, Specs-Flex Mode). The spectra of LrGO-Ag, LrGO-Cu_2O, LrGO-Ag-Cu_2O nanocomposites were observed by ultraviolet-visible spectroscopy (UV-Vis, Shimadzu-UV 1601) with a scan interval 200 nm to 900 nm at room temperature.

5. Catalytic Activity Studies

The reduction of 4-NP and MB was investigated using LrGO-

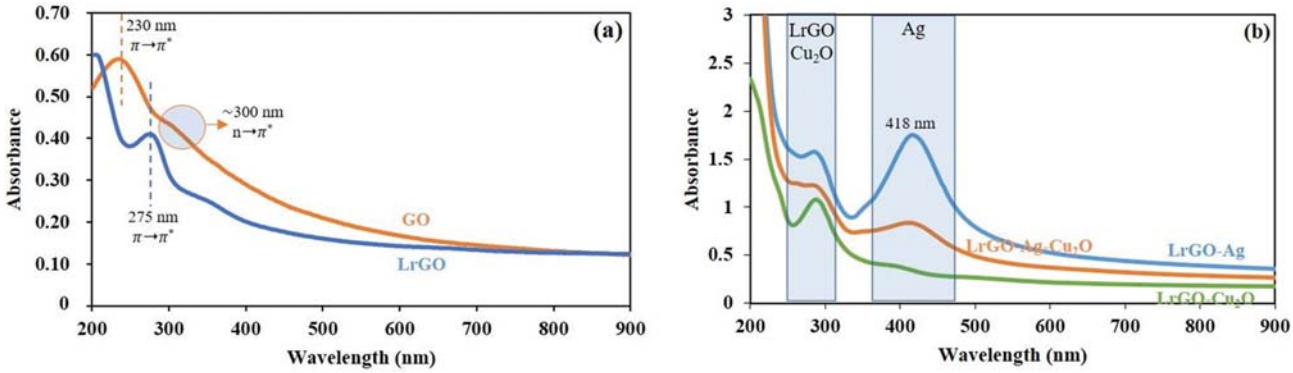

Fig. 2. UV-Vis spectra of (a) GO, LrGO (b) LrGO-Ag, LrGO-Cu_2O, LrGO-Ag-Cu_2O nanostructures.

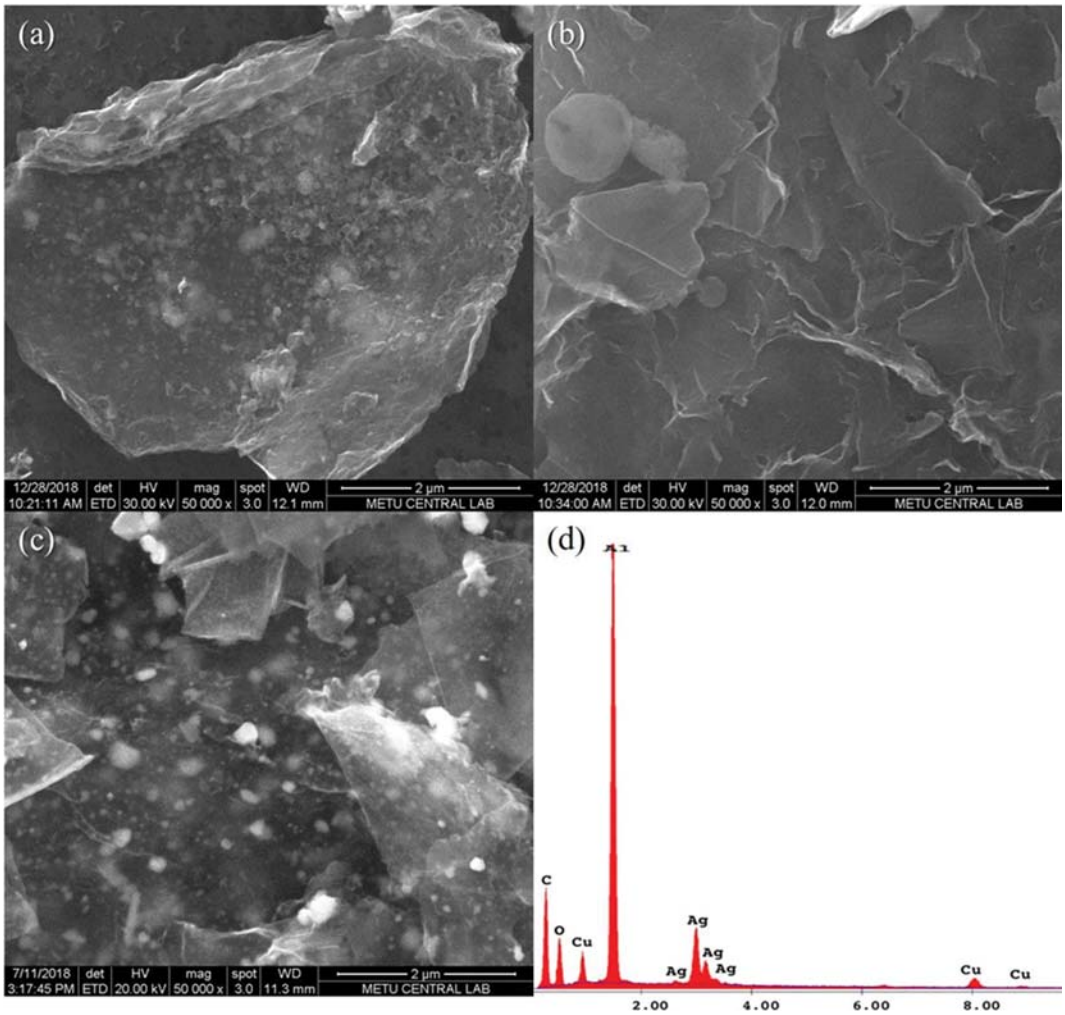

Fig. 3. SEM images of (a) LrGO-Ag, (b) LrGO-Cu_2O and (c) LrGO-Ag-Cu_2O nanocomposites (d) EDX spectrum of LrGO-Ag-Cu_2O nanocomposite.

Ag, LrGO-Cu_2O, LrGO-Ag-Cu_2O nanostructures as catalysts. 4-NP and MB solutions were prepared freshly at 9.6×10^{-5} mM and 4.8×10^{-5} mM concentrations, respectively. Excess amount of $NaBH_4$ (0.1 M and 0.48 ml) was added to the dye solutions. The final solutions (2.7 ml) were placed in a quartz cuvette and the reduction of 4-NP and MB was observed with the addition of 0.5 mg catalyst. The catalytic activity of LrGO-Ag, LrGO-Cu_2O, LrGO-Ag-Cu_2O nanocomposites was observed by UV-Vis in the range of 200 nm to 500 nm for reduction of 4-NP and 250 nm to 750 nm for reduction of MB at room temperature.

RESULTS AND DISCUSSION

1. Characterization of Synthesized Nanostructures

FTIR spectra of the *C. islandica* extract, GO, LrGO, LrGO-Cu_2O, LrGO-Ag, and LrGO-Ag-Cu_2O nanostructures are given in Fig. 1(a)-(e). The characteristic peaks of the *C. islandica* extract were observed at 3,387 cm^{-1} (O-H stretching vibration), 2,924 cm^{-1} and 2,854 cm^{-1} (C-H stretching vibrations of aliphatic acids), 1,743 cm^{-1} (C=O chain ester vibration), 1,697 cm^{-1} (C=O phenyl ester vibration), 1,651 cm^{-1} (C=O aldehyde vibration), 1,573 cm^{-1} (C=C vibration), 1,450 cm^{-1} (CH_2, CH_3 band), 1,273 cm^{-1} and 1,072 cm^{-1} (C-O methyl ester vibrations) (Fig. 1(a)). The absorption bands of O-H stretching vibration (3,402 cm^{-1}), C=O carboxyl stretching vibration (1,720 cm^{-1}), C-OH stretching vibration (1,383 cm^{-1}), C-O epoxy stretching vibration (1,219 cm^{-1}) and C-O alkoxy stretching (1,041 cm^{-1}) were attributed to oxygenated functional groups of GO. The peak at 1,620 cm^{-1} indicated skeletal vibrations of unoxidized graphite. Decreasing of the characteristic peak intensities of the oxide groups, proved the reduction of GO to LrGO (Fig. 1(b) and 1(c)). The presence of a peak at 617 cm^{-1} expressed the Cu-O stretching vibration in the structure of the LrGO-Cu_2O and LrGO-Ag-Cu_2O (Fig. 1(d) and 1(f)). The results are compatible with the literature [44-48].

Fig. 2 shows UV-Vis spectra of the GO and the synthesized nanostructures by *C. islandica* extract. The characteristic absorption peaks of GO at 230 nm and about 300 nm demonstrate the π-π* transitions of the aromatic C-C bonds and n-π* transitions of the C=O bonds, respectively. After the reduction of GO (LrGO), the maximum UV-Vis absorption band of π-π* transition redshifted from 230 nm to 275 nm (Fig. 2(a)). It was determined that the Ag nanoparticles had a characteristic surface plasmon resonance (SPR) band absorption at 418 nm. In the spectrum of the simultaneously reduced nanostructures included GO, $AgNO_3$ and $CuSO_4$, the SPR band of Ag nanoparticles, absorption band of Cu_2O nanoparticles, and π-π* transition band of LrGO were observed (Fig.

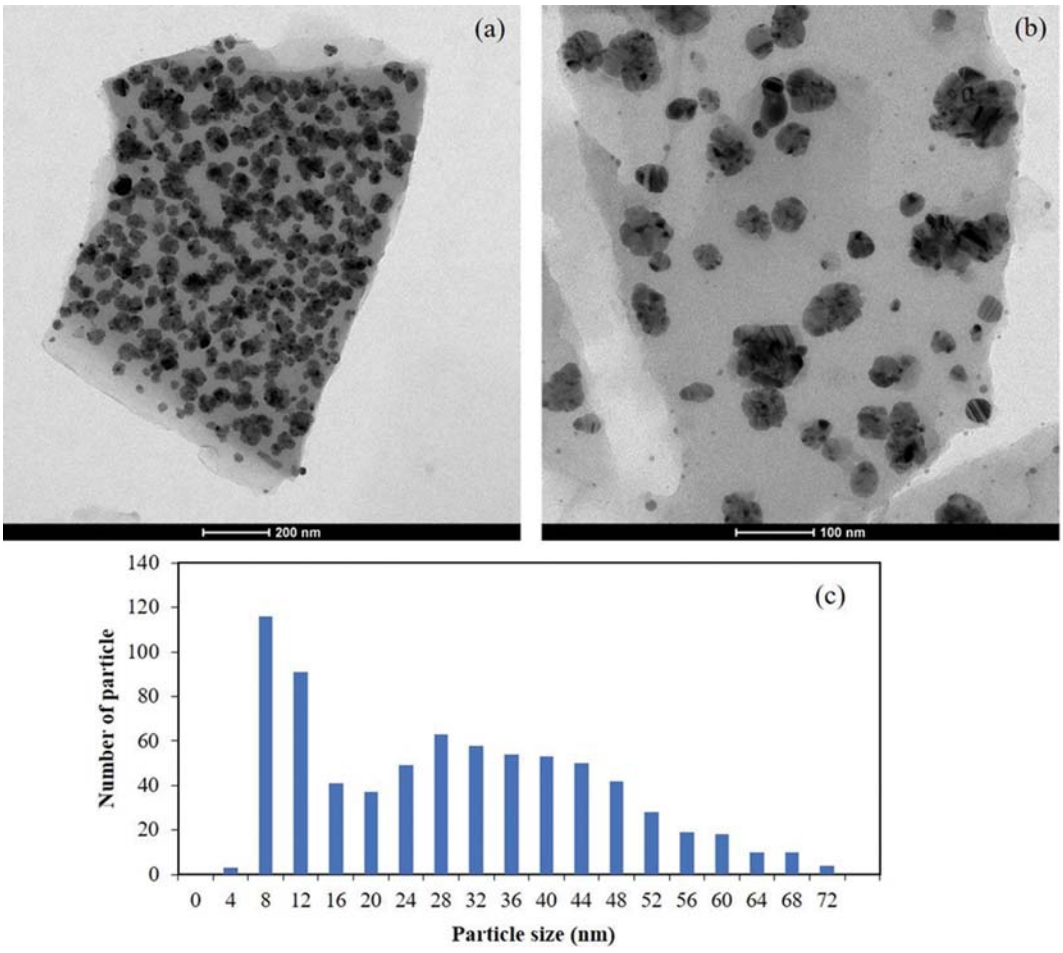

Fig. 4. (a), (b) TEM images, (c) particle size distribution of LrGO-Ag-Cu_2O nanocomposite.

2(b)). Similar results were seen in the literature [49-51]. UV-vis results indicate the successful preparation of Cu_2O and Ag nanoparticles on LrGO nanosheets.

SEM images of LrGO-Ag, LrGO-Cu_2O and LrGO-Ag-Cu_2O nanocomposites are shown in Fig. 3(a), 3(b), and 3(c), respectively. Nanoparticles were well dispersed on the LrGO nanosheets by the reducing and stabilizing effect of *C. islandica*. The result of EDX analysis seen in Fig. 3(d) verified the presence of Ag, Cu_2O and LrGO nanostructures due to the existance the peaks of Ag, Cu, O and C elements. That confirmed the prepared nanoparticles consisted of Ag and Cu_2O.

TEM images and the particle size distribution of LrGO-Ag-Cu_2O nanocomposites are given in Fig. 4. Combined spherical Ag and Cu_2O nanoparticles on the LrGO achieved by the simultaneous reduction of GO, $AgNO_3$, and $CuSO_4$ appear clearly in Fig. 4(a) and 4(b). The mean particle size of Ag-Cu_2O nanoparticles was determined as 27 nm from the particle size histogram having two

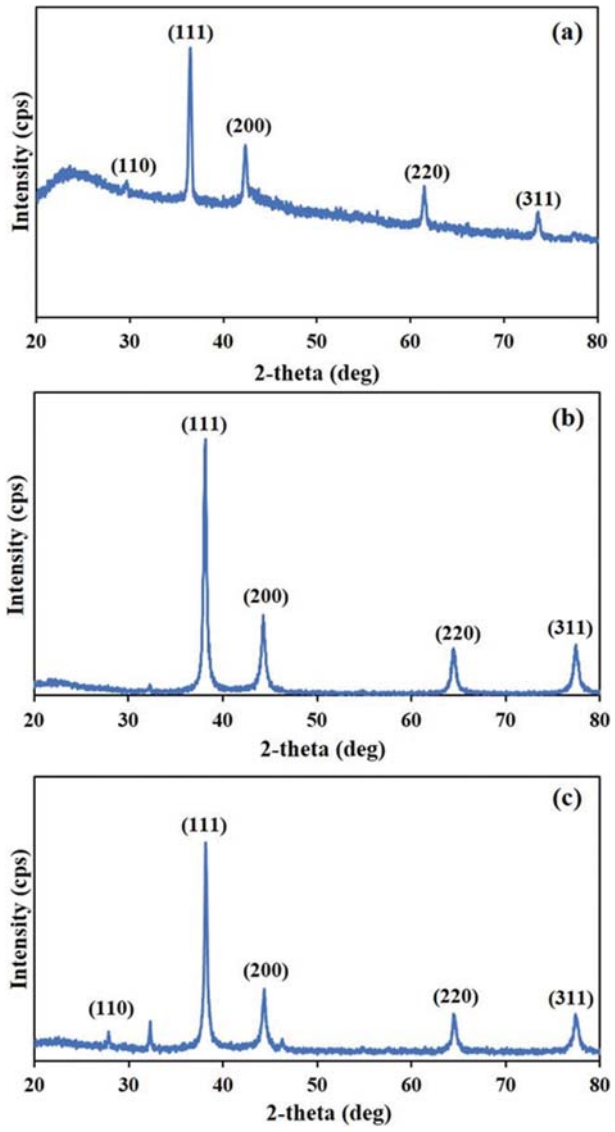

Fig. 5. XRD patterns of (a) LrGO-Cu_2O, (b) LrGO-Ag and (c) LrGO-Ag-Cu_2O nanocomposites.

fractional distribution (Fig. 4(c)). Stable nanoparticles which well scattered on the LrGO nanosheets were obtained with a narrow particle size distribution. SEM and TEM results proved that LrGO nanosheets are effective platforms for the preparation of stable Ag and Cu_2O nanoparticles because of their very high surface area.

Fig. 5 represents the XRD results of LrGO-Ag, LrGO-Cu_2O and LrGO-Ag-Cu_2O nanocomposites. The characteristic diffraction peak of LrGO was seen around 23° which is close to graphite in all three patterns that exhibit, *C. islandica* is an efficient agent for the reduction of GO. The characteristic peaks at 29.6°, 36.5°, 42.2°, 61.5°, 71.6° which belong to (110), (111), (200), (220) and (311) planes confirmed the presence of Cu_2O nanoparticles (Fig. 5(a)). In addition, Ag nanoparticles had peaks at 38.1°, 44.3°, 64.4°, 77.4° belonging to (111), (200), (220) and (311) crystal planes (Fig. 5(b)). The characteristic peaks of Ag, Cu_2O and LrGO also existed in the XRD pattern of LrGO-Ag-Cu_2O (Fig. 5(c)) [52-55].

XPS analysis was performed to determine the surface chemical composition of ternary LrGO-Ag-Cu_2O nanocomposite. Fig. 6(a) shows the XPS survey spectra of LrGO-Ag-Cu_2O sample. XPS survey spectra of LrGO-Ag-Cu_2O revealed the presence of C, O, Ag, and Cu atoms with photoelectron peaks of C 1s (284.2 eV), O 1s (532.6 eV), Ag 3d (466.6 eV), and Cu 2p (933.4 eV), respectively. The C 1s XPS spectrum of ternary nanocomposite consists of four peaks that correspond to carbon C-C bond (283.2 eV), epoxy/hydroxyl C-O (285.2 eV), carbonyl C=O (287.5 eV) and carboxylates O-C=O (289.2 eV), respectively (Fig. 6(b)) [56,57]. Despite reduced by lichen extract, the ternary nanocomposite has high content of oxygenated functional groups because of the presence of oxygen rich aromatic compounds of *C. islandica* extract, such as cetraric acid, fumarprotocetraric acid, and usnic acid. Fig 6(c) shows high-resolution Ag 3d XPS spectra of LrGO-Ag-Cu_2O nanocomposite. The Ag 3d XPS spectra of ternary nanocomposite consist of Ag $3d_{3/2}$ (372.8 eV) and Ag $3d_{5/2}$ (366.9 eV), which indicates the presence of Ag in the zero-valance state [57]. Fig. 6(d) shows the Cu 2p XPS spectra of ternary nanocomposite. The peaks at binding energy of 932.7 eV and 952.8 eV are ascribed to Cu $2p_{3/2}$ and Cu $2p_{5/2}$ peaks of Cu^+ bonds, respectively. Consistent with XRD results, XPS results show the presence of Cu_2O nanoparticles on LrGO nanosheets [58,59].

2. Catalytic Activity Studies

The catalytic activity of the synthesized nanostructures (LrGO-Cu_2O, LrGO-Ag, LrGO-Ag-Cu_2O) was investigated by 4-NP and MB reduction with $NaBH_4$. Catalytic reduction of the dyes is an electron transfer process. The large standard reduction potentials among 4-NP/4-AP (−0.76 V), MB/LMB (−1.33 V) and H_3BO_3/BH_4^- (−1.33 V) inhibit the progression of the MB and 4-NP reduction reactions with $NaBH_4$. To overcome this hindrance, MB and 4-NP reaction in the presence of $NaBH_4$ can be realized by addition of favorable catalyst to the reaction medium. After the adsorption of reducing agent (BH_4^-) and dye molecules (MB and 4-NP) on catalyst particle surfaces, a catalyst which has a very high surface area can supply electron transfer from the donor BH_4^- to the acceptors 4-NP/MB to catalyze the reaction [34,60-63].

UV-Vis characteristic absorption peaks of 4-NP and MB in the presence of $NaBH_4$ were at 400 nm (Fig. 7), 616 nm and 662 nm (Fig. 8), respectively. The decrease of the peak intensity indicated

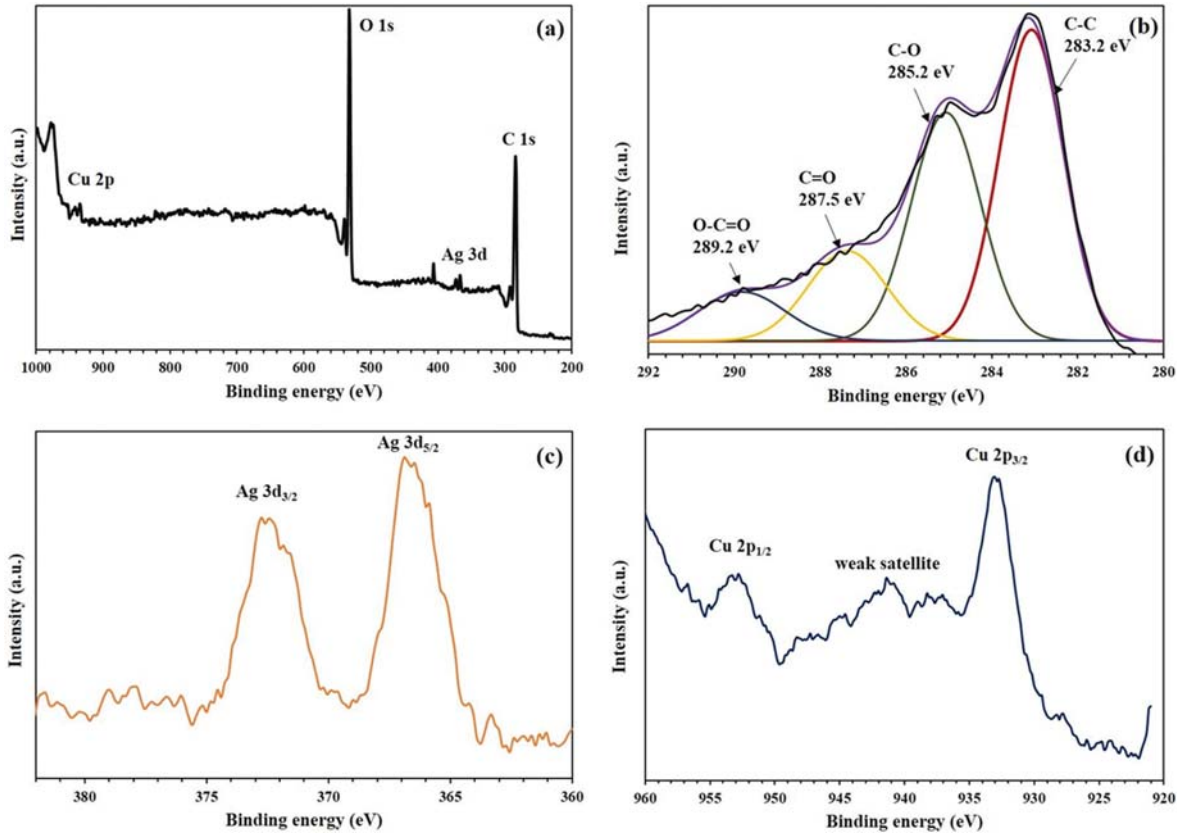

Fig. 6. (a) XPS survey spectra of LrGO-Ag-Cu_2O nanocomposite, (b) C1s, (c) Ag 3d, (d) Cu 2p XPS spectra of LrGO-Ag-Cu_2O nanocomposite.

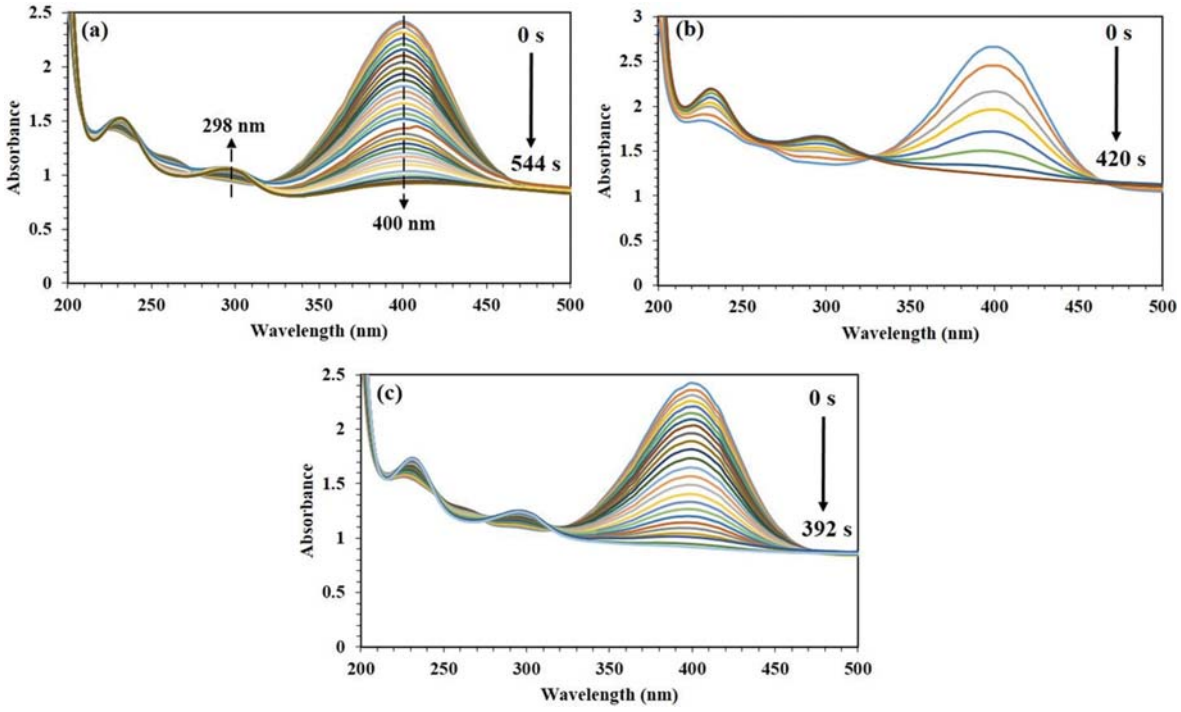

Fig. 7. UV-Vis spectra for catalytic reduction of 4-NP in the presence of $NaBH_4$ by (a) LrGO-Ag, (b) LrGO-Cu_2O and (c) LrGO-Ag-Cu_2O.

the catalytic reduction of the dyes. At the same time, new peaks related to reduction appeared in the UV-Vis spectrum. UV-Vis peaks at 298 nm and 292 nm were newly formed which belong to reduction products 4-AP and LMB. Before the investigation of

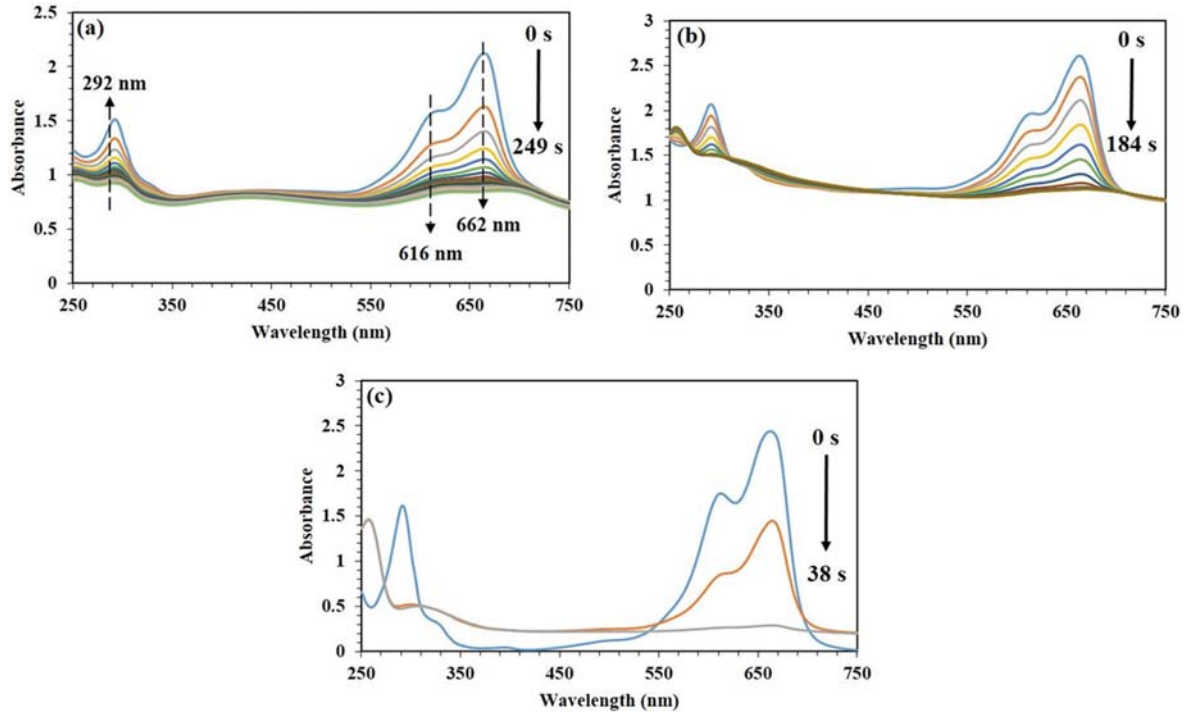

Fig. 8. UV-Vis spectra for catalytic reduction of MB in the presence of $NaBH_4$ by (a) LrGO-Ag, (b) LrGO-Cu_2O and (c) LrGO-Ag-Cu_2O.

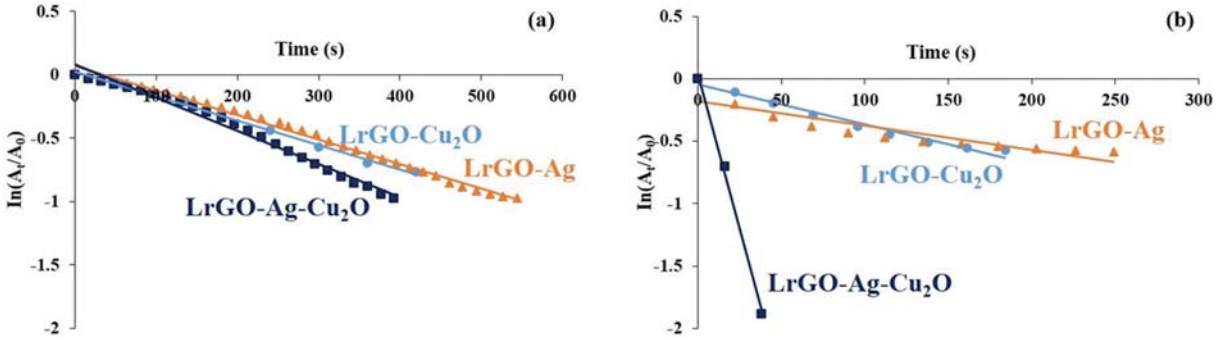

Fig. 9. The plot of $\ln(A_t/A_0)$ versus time for catalytic reduction of (a) 4-NP, (b) MB.

catalytic activity of nanoparticle decorated LrGO nanocomposites, the effects of LrGO and *C. islandica* extract on the reduction of 4-NP and MB were examined. The presence of neither LrGO nor *C. islandica* extract caused a change on the absorption peaks of 4-NP and MB even after hours, which verifies reduction of dyes is not possible without the addition of nanoparticle catalyst. The catalytic reduction of 4-NP and MB with LrGO-Ag, LrGO-Cu_2O and LrGO-Ag-Cu_2O nanostructures are given in Fig. 7 and Fig. 8, respectively.

Reaction rate constants (k, s^{-1}) were calculated based on the assumption of pseudo-first-order kinetics by the following equation:

$$\ln(A_t/A_0) = -kt \quad (1)$$

A_t and A_0 are the absorbances at time t and t=0, respectively. The graphics of $\ln(A_t/A_0)$ versus time were plotted for the catalytic reduction of 4-NP and MB. Fig. 9 shows the plot of $\ln(A_t/A_0)$ versus time for the catalytic reduction of 4-NP and MB with LrGO-Cu_2O, LrGO-Ag, LrGO-Ag-Cu_2O. The pseudo-first-order rate constants were calculated from slopes of the lines of $\ln(A_t/A_0)$ versus time plots [64-66]. All pseudo-first-order rate constants and the reduction durations for LrGO-Ag, LrGO-Cu_2O, LrGO-Ag-Cu_2O

Table 1. Pseudo-first-order rate constants (k, s^{-1}) and the reduction durations (s) with different catalysts

	4-NP		MB	
	k (s^{-1})	t (s)	k (s^{-1})	t (s)
Ag	0.0015	720	0.0019	480
Cu_2O	0.0013	825	0.0016	480
Ag-Cu_2O	0.0016	700	0.0042	420
LrGO-Ag	0.0019	544	0.0020	249
LrGO-Cu_2O	0.0019	420	0.0032	184
LrGO-Ag-Cu_2O	0.0026	392	0.0497	38

nanocomposites and Ag, Cu_2O, Ag-Cu_2O nanoparticles are given in Table 1.

When the catalytic activity of the nanocomposites on 4-NP was examined, the reaction rates were determined as 0.0019 s^{-1}, 0.0019 s^{-1} and 0.0026 s^{-1} for LrGO-Ag, LrGO-Cu_2O and LrGO-Ag-Cu_2O nanocomposites, respectively. Furthermore, the reaction durations decreased from 544 s (LrGO-Ag) to 392 s (LrGO-Ag-Cu_2O). Similarly, the catalytic reaction rates and reaction durations of MB reduction were found as 0.0020 s^{-1}, 0.0032 s^{-1}, 0.0497 s^{-1} and 249 s, 184 s and 38 s for LrGO-Ag, LrGO-Cu_2O and LrGO-Ag-Cu_2O, respectively (Table 1). The better catalytic activity depends on higher surface area and more active sites of the nanostructures for the specific dyes. On the other hand, due to the low electron density of pristine Cu_2O, Cu_2O nanostructures have very low catalytic activity towards the reduction of dye molecules. Combination of Cu_2O nanoparticles with LrGO nanosheets has high catalytic activity. Effective loading of Cu_2O nanoparticles having a small mean particle size with homogeneous coating of LrGO nanosheets results in increased active surface area of the catalyst. Moreover, the reduction of Cu_2O nanoparticles with excess amount of $NaBH_4$ during catalytic experiments leads to formation of Cu(0) species, which is highly active for the reduction of dye molecules. Because of this synergistic effect, LrGO-Cu_2O nanocomposite has high catalytic activity [21,67,68]. For LrGO-Ag binary nanocomposite, Ag nanoparticles with the small size and high surface area undertake the role of nanoelectrode that provide electron transfer between BH_4^- to the electrophile 4-NP/MB [61]. In addition, Ag nanostructures trigger further increase of electron density of Cu_2O and presence of Ag nanostructures with low particle size, facilitate formation of larger potential difference between catalyst and electrophile 4-NP/MB that provide occurrence of fast electron transfer. Having high electron density and fast electron transfer, LrGO-Ag-Cu_2O ternary nanocomposite exhibited better catalytic activity compared to binary LrGO-Ag and LrGO-Cu_2O nanocomposites [69,70].

Ag-Cu_2O nanoparticles were exhibited better catalytic activity compared to Ag and Cu_2O nanoparticles, similarly with the samples prepared on LrGO nanosheets because of improved electron density and fast electron transfer. As catalytic studies show, nanocomposite samples displayed improved catalytic performance compared to Ag, Cu_2O, Ag-Cu_2O, which prepared without using LrGO nanosheets as support material. Similarly with many studies in the literature, our study indicates using rGO as a support material provides high surface area for preparation of metal/metal oxide nanoparticles with low particle size and narrow particle size distribution, which increases the effective surface area of catalysts and available active sites. As an effective support material rGO nanosheets prevent aggregation, sintering or leaching of nanoparticles. The π-π interaction of rGO with 4-NP/MB increases the concentration of 4-NP/MB around catalyst nanoparticles. In addition LrGO nanosheets, reduce the amount of metal precursors that are used for cost-effective production of catalysts [71-73].

Homogeneous decoration of LrGO nanosheet surfaces with Cu_2O and Ag nanoparticles having the small mean particle sizes and very high surface which were both effective catalytic components for the reduction of 4-NP and MB further increased the catalytic performance of LrGO-Ag-Cu_2O nanocomposite. LrGO-Ag-Cu_2O exhibited the best catalytic activity (k=0.0497 s^{-1}, 38 s) in the conversion of MB to LMB according to obtained reaction rates and reaction durations. In this study, the catalytic activity results for 4-NP were determined compatible with the literature and for MB reduction superior results were obtained than the literature [69,74,75].

CONCLUSION

LrGO based nanostructures containing Ag and Cu_2O were simultaneously reduced and stabilized by *C. islandica* extract successfully. The results indicated that the extract of *C. islandica* was a superior reducing agent as well as a stabilizing agent to synthesize LrGO-Cu_2O, LrGO-Ag and LrGO-Ag-Cu_2O. Ag-Cu_2O nanoparticles well dispersed on the LrGO were obtained by non-toxic, low-cost and environmentally friendly method for the first time using a lichen extract. The biosynthesized nanostructures were used as catalyst during the reduction of 4-Nitrophenol (4-NP) and methylene blue (MB) dyes. The reaction rates and reaction durations of LrGO-Ag-Cu_2O nanocomposites towards 4-NP and MB were found as 0.0026 s^{-1}, 392 s; 0.0497 s^{-1}, 38 s, respectively. They exhibited effective catalytic activity for different types of textile dyes and can be used to eliminate water pollution, which is one of the important problems of the world.

ACKNOWLEDGEMENTS

In this study, chemical and analysis facilities provided by Ankara University Research Foundation (Project no: 17L0443003) were utilized. The authors are grateful for this contribution.

REFERENCES

1. T. Ito, Y. Shimada and T. Suto, *Water Resour. Ind.*, **20**, 46 (2018).
2. S. Srinivasan and S. K. Sadasivam, *J. Water Process Eng.*, **22**, 180 (2018).
3. L. G. M. Silva, F. C. Moreira, A. A. U. Souza, S. M. A. G. U. Souza, R. A. R. Boaventura and V. J. P. Vilar, *J. Clean. Prod.*, **198**, 430 (2018).
4. E. GilPavas, I. Dobrosz-Gómez and M. Á. Gómez-García, *J. Water Process Eng.*, **22**, 73 (2018).
5. Y. Xu, Z. Li, K. Su, T. Fan and L. Cao, *Chem. Eng. J.*, **341**, 371 (2018).
6. A. M. Herrera-González, M. Caldera-Villalobos and A. A. Peláez-Cid, *J. Environ. Manage.*, **234**, 237 (2019).
7. M. Maham, M. Nasrollahzadeh, S. M. Sajadi and M. Nekoei, *J. Colloid Interface Sci.*, **497**, 33 (2017).
8. J. Mangalam, M. Kumar, M. Sharma and M. Joshi, *Nano-Struct. Nano-Objects*, **17**, 58 (2019).
9. E. Yilmaz, Y. Tut, O. Turkoglu and M. Soylak, *J. Iran. Chem. Soc.*, **15**, 1721 (2018).
10. D. Wang and Y. Li, *Adv. Mater.*, **23**, 1044 (2011).
11. Z. Jin, M. Xiao, Z. Bao, P. Wang and J. Wang, *Angew. Chem.*, **124**, 6512 (2012).
12. M. Pang, Q. Wang and H. C. Zeng, *Chem.-Eur. J.*, **18**, 14605 (2012).
13. I. Roy, A. Bhattacharyya, G. Sarkar, N. R. Saha, D. Rana, P. P. Ghosh, M. Palit, A. R. Das and D. Chattopadhyay, *RSC Adv.*, **4**, 52044 (2014).
14. T. Ping, S. Mihua, S. Chengwen, W. Shuaihua and C. Murong, *Rare Metal Mat. Eng.*, **45**, 2214 (2016).

15. C. Wu, X. An, S. Gao and L. Su, *RSC Adv.*, **5**, 71259 (2015).
16. N. Meir, I. J. La Plante, K. Flomin, E. Chockler, B. Moshofsky, M. Diab, M. Volokh and T. Mokari, *J. Mater. Chem. A*, **1**, 1763 (2013).
17. X. H. Guo, J. Q. Ma and H. G. Ge, *Russ. J. Phys. Chem. A*, **89**, 1374 (2015).
18. L. Chen, M. Liu, Y. Zhao, Q. Kou, Y. Wang, Y. Liu, Y. Zhang, J. Yang and Y. M. Jung, *Appl. Surf. Sci.*, **435**, 72 (2018).
19. L. Dou, Y. Wang, Y. Li and H. Zhang, *Dalton Trans.*, **46**, 15836 (2017).
20. A. Chakravarty, K. Bhowmik, A. Mukherjee and G. De, *Langmuir*, **31**, 5210 (2015).
21. P. C. Rath, D. Saikia, M. Mishra and H. M. Kao, *Appl. Surf. Sci.*, **427**, 1217 (2018).
22. S. M. Roopan, T. V. Surendra, G. Elango and S. H. S. Kumar, *Appl. Microbiol. Biotechnol.*, **98**, 5289 (2014).
23. P. Dauthal and M. Mukhopadhyay, *Ind. Eng. Chem. Res.*, **55**, 9557 (2016).
24. K. Vijayaraghavan and T. Ashokkumar, *J. Environ. Chem. Eng.*, **5**, 4866 (2017).
25. N. Zikalala, K. Matshetshe, S. Parani and O. S. Oluwafemi, *Nano-Struct. Nano-Objects*, **16**, 288 (2018).
26. G. Sharma, A. Kumar, S. Sharma, M. Naushad, R. P. Dwivedi, Z. A. ALOthman and G. T. Mola, *J. King Saud. Univ. Sci.*, **31**, 257 (2019).
27. E. S. Olafsdottir and K. Ingólfsdottir, *Planta Med.*, **67**, 199 (2001).
28. N. Yıldız, Ç. Ateş, M. Yılmaz, D. Demir, A. Yıldız and A. Çalımlı, *Green Process. Synth.*, **3**, 259 (2014).
29. M. Xu, S. Heidmarsson, E. S. Olafsdottir, R. Buonfiglio, T. Kogej and S. Omarsdottir, *Phytomedicine*, **23**, 441 (2016).
30. R. Zhou, Y. Yang, S. Y. Park, T. T. Nguyen, Y. W. Seo, K. H. Lee, J. H. Lee, K. K. Kim, J. S. Hur and H. Kim, *Sci. Rep.*, **7**, 8136 (2017).
31. A. K. Geim and K. S. Novoselov, *Nat. Mater.*, **6**, 183 (2007).
32. M. Nurunnabi, K. Parvez, M. Nafiujjaman, V. Revuri, H. A. Khan, X. Feng and Y. K. Lee, *RSC Adv.*, **5**, 42141 (2015).
33. K. S. Divya, A. Chandran, V. N. Reethu and S. Mathew, *Appl. Surf. Sci.*, **444**, 811 (2018).
34. R. Mata, A. Bhaskaran and S. R. Sadras, *Particuology*, **24**, 78 (2016).
35. S. Mowry and P. J. Ogren, *J. Chem. Educ.*, **76**, 970 (1999).
36. R. Krishna, D. M. Fernandes, C. Dias, C. Freire, J. Ventura and E. Titus, *Mater. Today Proc.*, **3**, 2814 (2016).
37. R. Prasad, M. K. Lolakshi and B. R. Bhat, *Synthetic Met.*, **219**, 26 (2016).
38. M. Nasrollahzadeh, M. Atarod, B. Jaleh and M. Gandomirouzbahani, *Ceram. Int.*, **42**, 8587 (2016).
39. M. Atarod, M. Nasrollahzadeh and S. M. Sajadi, *J. Colloid Interface Sci.*, **465**, 249 (2016).
40. L. Rout, A. Kumar, R. S. Dhaka, G. N. Reddy, S. Giri and P. Dash, *Appl. Catal. A Gen.*, **538**, 107 (2017).
41. L. Nirumand, S. Farhadi and A. Zabardasti, *Acta Chim. Slov.*, **65**, 919 (2018).
42. Z. Çıplak, B. Getiren, C. Gökalp, A. Yıldız and N. Yıldız, *Chem. Eng. Commun.*, **207**, 559 (2020).
43. X. Yuan, S. Xiao and T. N. Taylor, *Science*, **308**, 1017 (2005).
44. B. Haghighi and M. A. Tabrizi, *RSC Adv.*, **3**, 13365 (2013).
45. L. Wu, P. Qu, R. Zhou, B. Wang and S. Liao, *High Perform. Polym.*, **27**, 486 (2015).
46. Y. Guo, H. Wang, X. Ma, J. Jin, W. Ji, X. Wang, W. Song, B. Zhao and C. He, *ACS Appl. Mater. Interfaces*, **9**, 19074 (2017).
47. Z. Çıplak, C. Gökalp, B. Getiren, A. Yıldız and N. Yıldız, *Green Process. Synth.*, **7**, 433 (2018).
48. Z. Zhao, Z. Cai, L. Yang, Z. Hu, Y. Zhang, X. Peng, Q. Wang, X. Yuan and G. Li, *J. Mater. Sci. Mater. Electron.*, **29**, 17743 (2018).
49. K. Gopalakrishnan, C. Ramesh, M. Elango and M. Thamilselvan, *ISRN Mater. Sci.*, **2014**, 1 (2014).
50. M. Khan, A. H. Al-Marri, M. Khan, M. R. Shaik, N. Mohri, S. F. Adil, M. Kuniyil, H. Z. Alkhathlan, A. Al-Warthan, W. Tremel, M. N. Tahir and M. R. H. Siddiqui, *Nanoscale Res. Lett.*, **10**, 281 (2015).
51. T. K. Das, P. Bhawal, S. Ganguly, S. Mondal and N. C. Das, *Surf. Interface*, **13**, 79 (2018).
52. C. C. Yeh, P. R. Wu and D. H. Chen, *Mater. Lett.*, **136**, 274 (2014).
53. S. P. Dubey, T. T. Nguyen, Y. N. Kwon and C. Lee, *J. Ind. Eng. Chem.*, **29**, 282 (2015).
54. K. Sharma, K. Maiti, N. H. Kim, D. Hui, J. H. Lee, *Compos. Part B Eng.*, **138**, 35 (2018).
55. J. Pang, W. Li, Z. Cao, J. Xu, X. Li and X. Zhang, *Appl. Surf. Sci.*, **439**, 420 (2018).
56. P. A. Bozkurt, *Ultrason. Sonochem.*, **35**, 397 (2017).
57. Y. Zhang, J. Wang, J. Qiu, X. Jin, M. M. Umair, R. Lu, S. Zhang and B. Tang, *Appl. Energy*, **237**, 83 (2019).
58. W. Zhang, X. Li, Z. Yang, X. Tang, Y. Ma, M. Li, N. Hu, H. Wei and Y. Zhang, *Nanotechnology*, **27**, 265703 (2016).
59. W. Zhang, Z. Yin, A. Chun, J. Yoo, G. Diao, Y. S. Kim and Y. Piao, *J. Power Sources*, **318**, 66 (2016).
60. K. S. Shin, J. H. Kim, I. H. Kim and K. Kim, *J. Nanopart. Res.*, **14**, 735 (2012).
61. N. Isa and Z. Lockman, *Environ. Sci. Pollution R.*, **26**, 11482 (2019).
62. S. Hamedi, S. A. Shojaosadati and A. Mohammadi, *J. Photochem. Photobiol.*, **167**, 36 (2017).
63. E. Yilmaz and M. Soylak, *J. Iran. Chem. Soc.*, **14**, 2503 (2017).
64. K. C. Hsu and D. H. Chen, *Nanoscale Res. Lett.*, **9**, 484 (2014).
65. A. Ahmad, Y. Wei, F. Syed, M. Imran, Z. U. H. Khan, K. Tahir, A. U. Khan, M. Raza, Q. Khan and Q. Yuan, *RSC Adv.*, **5**, 99364 (2015).
66. M. Atarod, M. Nasrollahzadeh and S. M. Sajadi, *RSC Adv.*, **5**, 91532 (2015).
67. C. Huang, W. Ye, Q. Liu and X. Qiu, *ACS Appl. Mater. Interfaces*, **6**, 14469 (2014).
68. A. K. Sasmal, S. Dutta and T. Pal, *Dalton Trans.*, **45**, 3139 (2016).
69. S. Kandula and P. Jeevanandam, *Eur. J. Inorg. Chem.*, **2016**, 1548 (2016).
70. Z.-J. Jiang, C.-Y. Liu and L.-W. Sun, *J. Phys. Chem. B*, **109**, 1730 (2005).
71. J.-J. Lv, A.-J. Wang, X. Ma, R.-Y. Xiang, J.-R. Chen and J.-J. Feng, *J. Mater. Chem. A*, **3**, 290 (2015).
72. W. Ye, J. Yu, Y. Zhou, D. Gao, D. Wang, C. Wang and D. Xue, *Appl. Catal. B Environ.*, **181**, 371 (2016).
73. X. Li, Y. Ma, Z. Yang, D. Huang, S. Xu, T. Wang, Y. Su, N. Hu and Y. Zhang, *J. Alloys Compd.*, **706**, 377 (2017).
74. T. J. I Edison and M. G. Sethuraman, *Process Biochem.*, **47**, 1351 (2012).
75. S. H. Adyani and E. Soleimani, *Int. J. Hydrogen Energy*, **44**, 2711 (2019).